Detection of Wave Groups in SAR Images and Radar-Image Sequences

Heiko Dankert, Jochen Horstmann, Susanne Lehner, *Member, IEEE*, and Wolfgang Rosenthal

Abstract— **The properties of individual wave groups in space and time utilizing synthetic aperture radar (SAR) images and nautical radar-image sequences are studied. This is possible by the quantitative measurement and analysis of wave groups both spatially and spatial-temporally. The SAR, with its high spatial resolution and large coverage, offers a unique opportunity to study and derive wave groups. In addition to SAR images, nautical radar-image sequences allow the investigation of wave groups in space and time and therefore the measurement of parameters such as the group velocity. The detection of wave groups is based on the determination of the envelope function, which was first adopted for one-dimensional (1-D) time series by Longuet-Higgins. The method is extended from 1-D to spatial and spatio-temporal dimensions to derive wave groups in images and image sequences. To test the algorithm, wave groups are derived from SAR images and two radar-image sequences, recorded at locations in deep and shallow water. It is demonstrated that the algorithm can be employed for the determination of both location and size of wave groups from radar images. Investigating the detected wave groups in radar-image sequences additionally allows the measurement of the spatial and temporal development of wave groups and their extension and phase velocities. Comparison of measured wave group velocities in shallow and deep water gives a deviation of the average value from the group velocities resulting from linear wave theory and shows a clear oscillation of the group velocities in 2d.**

Keywords—**wave groups, group velocity, rogue waves, nautical radar, synthetic aperture radar**

I. Introduction

WAVE GROUPS play an important role for the design and assessment of offshore-platforms, breakwaters or ships, because successive large single wave crests or deep troughs can cause severe damages due to their impact, or they can excite the resonant frequencies of the structures. For ships, an encounter with wave groups can sometimes cause capsize or severe damage. An extreme wave can develop from a large wave group due to interference of its harmonic components [1]. Therefore the detection of wave groups in space and time is of extreme importance for ocean engineers and scientists.

In our mathematical description wave groups are the result of superposition of elementary wave components (e.g. sinusoidal waves) moving in similar direction with slightly different wave lengths and periods. The groups on the ocean surface, characterized by amplitudes above a threshold, move with their own group velocity. The group velocity is important because wave energy is propagated with this velocity. In deep water the speed of individual crests and troughs is called phase speed and is usually greater than group velocity. For a sinusoidal wave with wave number k and frequency ω the phase speed is described by $C = \omega/k$. The group velocity for a superposition of sinusoidal waves with slightly different frequencies and wave numbers is $C_g = \partial\omega/\partial k$, the gradient of the dispersion relation of linear surface-gravity waves. This mathematical idealized group velocity for a narrow spectrum is not valid for all types of observed wave groups. We will show in chapter V wave groups on the ocean that move with different velocities.

Wave groups have already been studied on 1d-data sets from wave recorders. Thereby the sea surface elevation is measured in situ at one fixed point over time. Longuet-Higgins [2],[3] was one of the first to investigate wave groups by considering the wave envelope. In this work the main assumptions are that the sea surface is considered a Gaussian process and the frequency spectrum consists of a single narrow frequency band. Only in the latter case can wave groups be meaningful defined. For a wide-banded frequency spectrum the organized movement of waves is less noticeable and the concept of a carrier wave is not useful. Each large wave could be taken as a crest of a wave group.

The limitation of considering the sea surface over time at fixed points in space can be overcome by measuring with imaging devices. We concentrate in this work on radar images. The European satellites ERS-1, ERS-2 and recently ENVISAT, continuously record images of the ocean surface with a synthetic-aperture radar (SAR) from a near-circular, polar and sun-synchronous orbit at a mean altitude of 785 km. Thereby the radar backscatter from the ocean surface, called sea clutter, is modulated by the long surface waves. The imaging mechanisms are basically well understood [4], [5] so that it is possible to study the behavior of the ocean gravity waves with this instrument. The ERS-SAR acquires images with a size of approximately 100 m $\times$ 100 m with a spatial resolution of $\approx$ 25 m in range (antenna look direction) and 6 to 30 m in an azimuthal direction (flight direction). It operates at a frequency of 5.3 GHz (C-band) and transmits and receives with linear vertical polarization at incidence angles between 20° and 26°.

SAR intensity images are single images and contain no information on wave travel direction. But as in SAR images every scattering point of the sea surface is illuminated for about 0.7 seconds phase information of single look com-

Manuscript received September 23, 2002; revised February 19, 2003.

This work was supported by the European project MAXWAVE Project evk: 3-2000-00 544.

H. Dankert, J. Horstmann and W. Rosenthal are with the GKSS Research Center, 21502 Geesthacht, Germany

S. Lehner is with the German Aerospace Center (DLR), 82234 Oberpfaffenhofen, Germany

Digital Object Identifier 10.1109/TGRS.2003.811815

plex (SLC) data can be used to select subintervals of this integration time, creating different images of coarser spatial resolution with a time difference of about 0.5 s. By computing the cross spectrum of the two images, the direction of the wave movement can be determined [6].

To capture a time series of ocean wave movement image sequences from a real aperture radar (RAR) can be utilized to overcome the directional limitation of single images. Young et al. [7] showed that it is possible to use a nautical radar to extract spectral information on the ocean surface wave field from the modulated backscatter of microwaves. For this purpose the Wave Monitoring System (WaMoS) based on a nautical radar was developed at GKSS Research Center [8], [9], which allows for digitization of time series of polar nautical radar images. The nautical radar operates at 9.5 GHz (X-band) with horizontal and vertical polarization in transmitting and receiving near grazing incidence [10]. It covers an area within a radius of about 2 km. The polar images are converted to rectangular coordinates. The grid size is chosen to be equal to the radar resolution of $\approx$ 10 m. The number of analyzed radar images is basically unlimited, but 32 are sufficient for operational purposes, such as the determination of 2d-wave spectra and sea state parameters. With an antenna-rotation time of about 2 s it takes therefore about 1 minute to record a data set. Should a method exist enabling the detection of extreme wave groups in radar-image sequences, safety programs could be started before a dangerous group could reach an oil-platform. Nautical radars for wave detection are operated on several towers in the North Sea, e.g. on the Norwegian Oil Platform "Ekofisk" and in the shallow water area at the island of Helgoland. Furthermore in the framework of the European project "MaxWave" data were recorded aboard a multipurpose container vessel sailing between Northern Europe and South Africa, passing the Aghulas Current, with strong wave-current interactions.

We emphasize in this paper the distribution and the properties of individual wave groups in space for typical sea states that are usually defined by statistical quantities like the significant wave height H_S, peak frequency f_P, directional spread etc.. An algorithm is developed and tested utilizing SAR images and nautical radar-image sequences. The wave groups from radar-image sequences are further investigated regarding their measured group velocity in comparisation with the theoretical group velocity.

II. Derivation of spatio-temporal Wave Envelope

Wave groups are the result of interference of wave components moving in similar direction with slightly different periods. The group properties of a wave record of the sea-surface elevation in time at one location can be described with its wave envelope function [2], [11], [12]. If a carrier wave can be found in the signal, the wave envelope is always defined by the local and temporal amplitude and phase. Thereby mathematically the carrier wave can always be defined as a wave with wave number $\bar{\vec{k}}$ and angular frequency $\bar{\omega}$ from the coefficients of the variance spectrum [2].

To retrieve 3d-wave groups (two horizontal space dimensions, one time dimension) in the spatio-temporal domain the 3d-wave envelope has to be determined. The sea-surface elevation $\eta(\vec{r}, t)$ at a location $\vec{r} = (x, y)$ and time t for a finite area of size $L_x \times L_y$ and a finite time interval T can be expressed locally as the product of a complex envelope function $\hat{\rho}(\vec{r}, t)$, the analytic signal of the real valued $\eta(\vec{r}, t)$ respectively, centered on the wave number and angular frequency of the carrier wave $(\bar{\vec{k}}, \bar{\omega})$, and a carrier wave:

$$\eta = \Re e \hat{\rho}(\vec{r}, t) e^{i(\bar{\vec{k}} \cdot \vec{r} - \bar{\omega} t)}, \tag{1}$$

with

$$\begin{aligned} \hat{\rho}(\vec{r}, t) &= \rho(\vec{r}, t) e^{i\phi(\vec{r}, t)} = \sum_{m=-\frac{N_x}{2}}^{\frac{N_x}{2}-1} \sum_{n=-\frac{N_y}{2}}^{\frac{N_y}{2}-1} \sum_{\tau=-\frac{N_T}{2}}^{\frac{N_T}{2}-1} \\ & \xi(\vec{k}_{(m,n)}, \omega_\tau) e^{i[(\vec{k}_{(m,n)} - \bar{\vec{k}}) \cdot \vec{r} - (\omega_\tau - \bar{\omega}) \cdot t]}, \end{aligned}$$

where $k_{xm} = \frac{2\pi m}{L_x}$, $k_{yn} = \frac{2\pi n}{L_y}$ and $\omega_\tau = \frac{2\pi\tau}{T}$. $N_{(x,y)}$ are the number of points of the rows and columns in the images and N_T gives the number of images. The wave-number vector is $\vec{k} = (k_x, k_y)$. $\hat{\rho}(\vec{r}, t)$ is defined by the wave crests, where it is determined by the wave elevation or by the square root of the potential energy E_p. The vertical velocity $w(\vec{r}, t)$ for each component is shifted relative to the amplitude by a phase of $\pi/2$. At the wave crests $\eta(\vec{r}, t)$ has its maximum and the phase $\phi = 0$. $w(\vec{r}, t)$ for each component of $\hat{\rho}(\vec{r}, t)$ vanishes at these points and therefore the kinetic energy E_k is zero. $\rho(\vec{r}, t)$ is the real envelope function of $\eta(\vec{r}, t)$, which is the modulus of the analytic function $\hat{\rho}(\vec{r}, t)$.

With the given real valued image sequence and its Fourier transform $F(\vec{k}, \omega)$, the complex envelope function $\hat{\rho}(\vec{r}, t)$ is defined by

$$\begin{aligned} \hat{\rho}(\vec{r}, t) &= 2 \sum_{m=-\frac{N_x}{2}}^{\frac{N_x}{2}-1} \sum_{n=-\frac{N_y}{2}}^{\frac{N_y}{2}-1} \sum_{\tau=0}^{\frac{N_T}{2}-1} \\ & F(\vec{k}_{(m,n)}, \omega_\tau) e^{i[\vec{k}_{(m,n)} \cdot \vec{r} - \omega_\tau \cdot t]}, \end{aligned}$$

which is just the inverse (discrete) Fourier transform of the positive frequency part of $F(\vec{k}, \omega)$. It is likewise which frequency domain is selected since $F(\vec{k}, \omega)$ is a Hermitian function. The Fourier transform $\hat{F}(\vec{k}, \omega)$ of $\hat{\rho}(\vec{r}, t)$ is given by

$$\hat{F}(\vec{k}, \omega) = 2u(\omega) F(\vec{k}, \omega). \tag{2}$$

where $u(\omega)$ denotes the Heaviside unit step function:

$$u(\omega) := \begin{cases} 1 & if \quad \omega > 0 \\ 0 & if \quad \omega < 0 \end{cases} \tag{3}$$

To get a smoother envelope, one has to filter out the higher frequency components in the record, while on the other hand, wave components with frequencies much lower then those of the dominant waves (the mean sea surface level is generally not of interest) can be neglected. This can be done in a preprocessing step. Longuet-Higgins [3] for instance filtered out the high and low frequencies. Practically, the data set is transformed into the fourier domain with a Fourier transformation and a bandpass-filter is applied to the complex Fourier coefficients for the chosen low and high cut-off frequencies.

This method for determining the envelope function can be applied to single images as well. Because of the axis dependency of the Hilbert transform in space dimensions, the elimination of the conjugate part of the Fourier coefficients in the wave-number spectrum for multi-modal wave fields can be ambiguous as the spectral peaks of the overlaying wave systems could overlap. The problem can be resolved by introducing a virtual frequency domain using the dispersion relation of linear surface-gravity waves, which is discussed later. The function is connecting the wave-number and frequency coordinates. In this way the wave-number frequency domain can be virtually constructed and the individual modes are separable.

For the time development of the sea surface elevation one may look for wave groups that propagate with a shape that is not changing in time. This means that $\hat{\rho}(\vec{r},t)$ moves with a constant velocity $\vec{v}_G$ and has the shape

$$\hat{\rho}(\vec{r},t) = \tilde{\rho}(\vec{r} - \vec{v}_G t). \tag{4}$$

$\vec{v}_G$ is not necessarily the theoretical one dimensional group velocity $\partial\omega/\partial k$.

III. Algorithm

The scheme of the complete algorithm is described as follows and is shown in Fig. 1. A given record of an image sequence $G(x,y,t)$ is first transformed into the wave-number frequency domain with a 3d Fast-Fourier Transformation (FFT), resulting in a complex 3D-image spectrum:

$$\hat{F}(k_x,k_y,\omega) = \sum_{x,y,t} G(x,y,t) e^{-i(k_x x + k_y y - \omega t)} \tag{5}$$

The signal of linear surface-gravity waves is well-located on a surface in the wave-number frequency domain defined by the dispersion relation of linear surface-gravity waves [7], [13]:

$$\omega^2 = gk \tanh kd \tag{6}$$

where g is the gravitational acceleration and d the water depth. The so-called dispersion shell connects the wave-number coordinates $\vec{k}$ with their corresponding frequency coordinate ω (see also Fig. 2). This function is used for a pre-selection of the Fourier coefficients in the spectrum of a multimodal wave field with image features that are not resulting from ocean surface waves.

To retrieve a smooth envelope, a bandpass-filter is used to select the Fourier coefficients around the spectral peak and suppress noise from non-relevant spectral components. This is performed by a normalized 3D-Gabor filter which has the advantage of reducing the filtering effects in temporal and spatial domain. A certain wave-number range

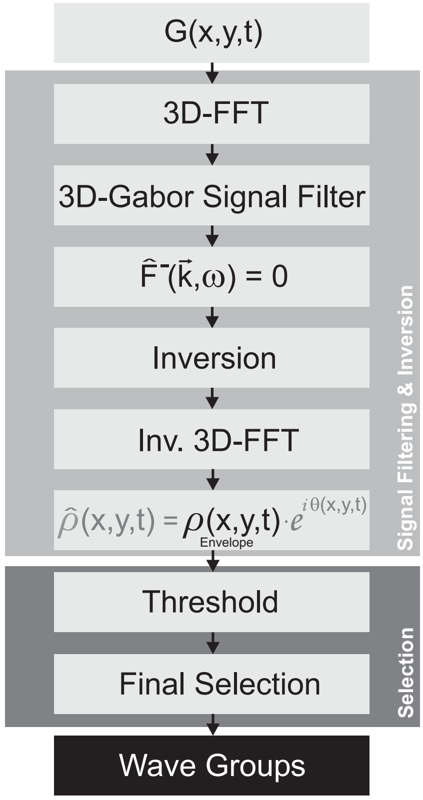

Fig. 1. Scheme of the Algorithm.

and frequency-range around the peak wave-number k_0 and peak frequency ω_0 is selected using a Gaussian function:

$$\hat{\Omega}(k_x,k_y,\omega) = e^{-\pi(|k_x-k_{x0}|^2\sigma_{k_x} + |k_y-k_{y0}|^2\sigma_{k_y} + |\omega-\omega_0|^2\sigma_\omega)} \tag{7}$$

where σ_{k_x}, σ_{k_y} and σ_ω are the standard deviations that define the filter bandwidth in the corresponding dimensions. The filter is similar to a windowed Fourier transformation with the Gaussian function as window function. In case there are several overlapping wave systems, a segmentation has to be performed. This can be done in the way introduced above or by applying the 3D-Garbor filter to every significant peak in the spectrum of the dominating wave systems.

The 3D-Gabor filter is multiplied with the complex Fourier coefficients of the wave-number frequency spectrum. The remaining spectrum consists only of the dominant harmonics around the spectral peak as indicated in Fig. 2. To retrieve the complex envelope function of the remaining signal the complex Fourier coefficients with negative frequencies $\hat{F}^-(\vec{k},\omega)$ are eliminated from the spectrum.

In the next step of the algorithm, an inversion technique is applied to the image spectrum $\hat{F}(\vec{k},\omega)$ to obtain the ocean wave field [14]. The spectral amplitudes of the image spectrum $\mathcal{I}(\vec{k},\omega)$ (the variance spectrum of grey levels) and the ocean wave spectrum $\mathcal{E}(\vec{k},\omega)$ (the variance spectrum of surface heave) are connected by an image transfer function

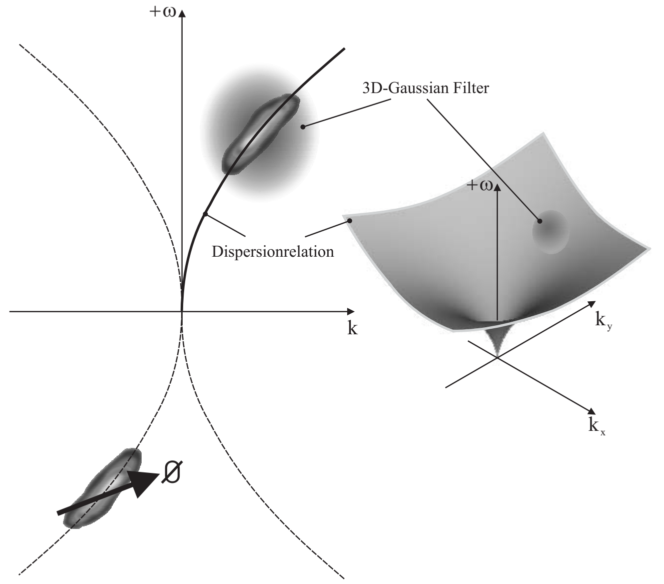

Fig. 2. The dispersion relation is used for a pre-selection of the Fourier coefficients in the spectrum of a multimodal wave field with image features that are not resulting from ocean surface waves. After multiplying of the 3D-Gabor filter with the complex Fourier coefficients of the wave-number frequency spectrum the remaining spectrum consists only of the dominant harmonics around the spectral peak. The complex envelope function of the remaining signal is determined by eliminating the negative frequencies from the spectrum.

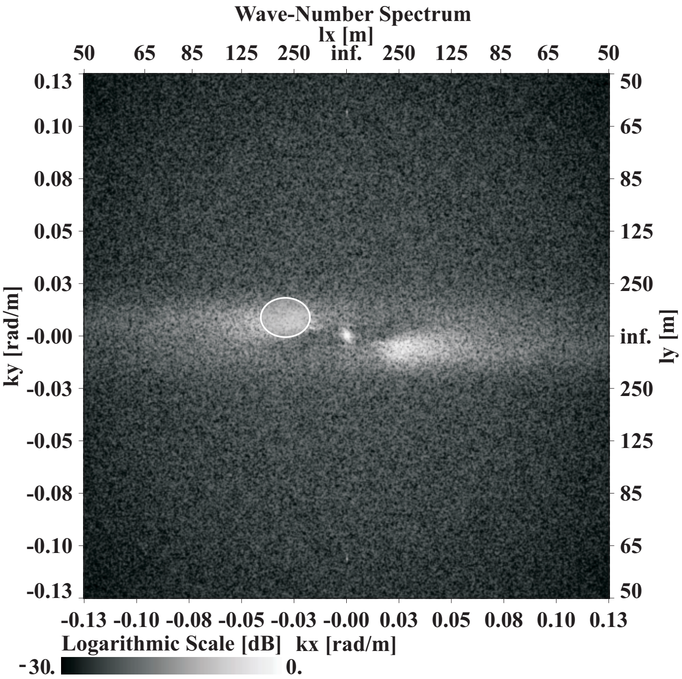

Fig. 3. Variance of the wave-number spectrum. The complex Fourier coefficients are filtered using a 2D-Gabor filter as band-pass filter, which is indicated by the white ellipse.

$\mathcal{M}(\vec{k})$:

$$\mathcal{I}(\vec{k}, \omega) = |\mathcal{M}(\vec{k})|^2 \mathcal{E}(\vec{k}, \omega), \tag{8}$$

where $\mathcal{M}(\vec{k})$ is parameterized as power law

$$|\mathcal{M}(\vec{k})|^2 = \alpha |\vec{k}|^{\beta}. \tag{9}$$

The exponent β has been retrieved by studying modulation effects like tilt modulation and shadowing. Thereby, Seemann [13] found shadowing the dominant modulation mechanism at grazing incidence, which gives $\beta \approx 1.2$. The calibration constant α is retrieved by comparison of the spectral zero-order moment of the image spectrum with in-situ measurements of the significant wave height.

After applying a 3D inverse Fourier transformation, the complex envelope of the wave field is determined in the spatial and temporal domain. To retrieve the dominant wave groups the modulus of the complex envelope, the amplitude, is filtered by simply thresholding. The obtained group areas are analyzed in regard to their area size, length and number of waves in a group. These parameters are used to discriminate between the groups for a final selection.

If the spectrum is wide-banded, the filtered frequency range of the bandpass filter has to be re-adjusted. The retrieved envelope will not be as smooth and maybe more difficult to analyze.

IV. Results from Single Radar Images

Two kinds of radar images were chosen to analyze wave groups. The first is a SAR image that was acquired on September 26, 1995, at the south-west coast of Norway by the satellite ERS-1. Fig. 4 shows the image with dimensions of about 100 km × 100 km. In the selected subimage, with a size of about 12.8 km × 12.8 km, a range travelling wave system is visible. The authors want to concentrate here on spatial and temporal distribution of wave envelopes and therefore the grey-level images instead of ocean topography are discussed. The nonlinearities of the SAR imaging effects such as velocity bunching and acceleration smearing are neglected [5], [15], [16] and the authors rely on a quasi-linear approximation. The resolution of ≈30 m has the same effect as a low pass filter so that only waves longer than ≈90 m are imaged by the SAR. To retrieve wave groups, the image is processed according to the algorithm.

Fig. 3 shows the variance spectrum of the Fourier transformed image with range and azimuth wave numbers, k_x and k_y respectively. The corresponding wave lengths l_x and l_y are plotted on the right and top. The intensity of the spectral amplitude is normalized to the intensity of the spectral peak of the filtered wave systems to highlight them. For retrieval of the complex envelope function, one of the point-symmetric spectral peaks is chosen using a 2D-Gabor filter, as indicated by the white ellipse in Fig. 3. The remaining complex Fourier coefficients are back-transformed by an inverse 2D-Fast Fourier Transform (FFT). The dominant wave groups are selected by thresholding the amplitude of the spatial determined wave envelope and by selecting only wave groups with a area size of at least 550 m × 550 m.

In Fig. 4 a SAR-sub image is depicted. Transparently overlayed are the wave envelopes of the selected dominant

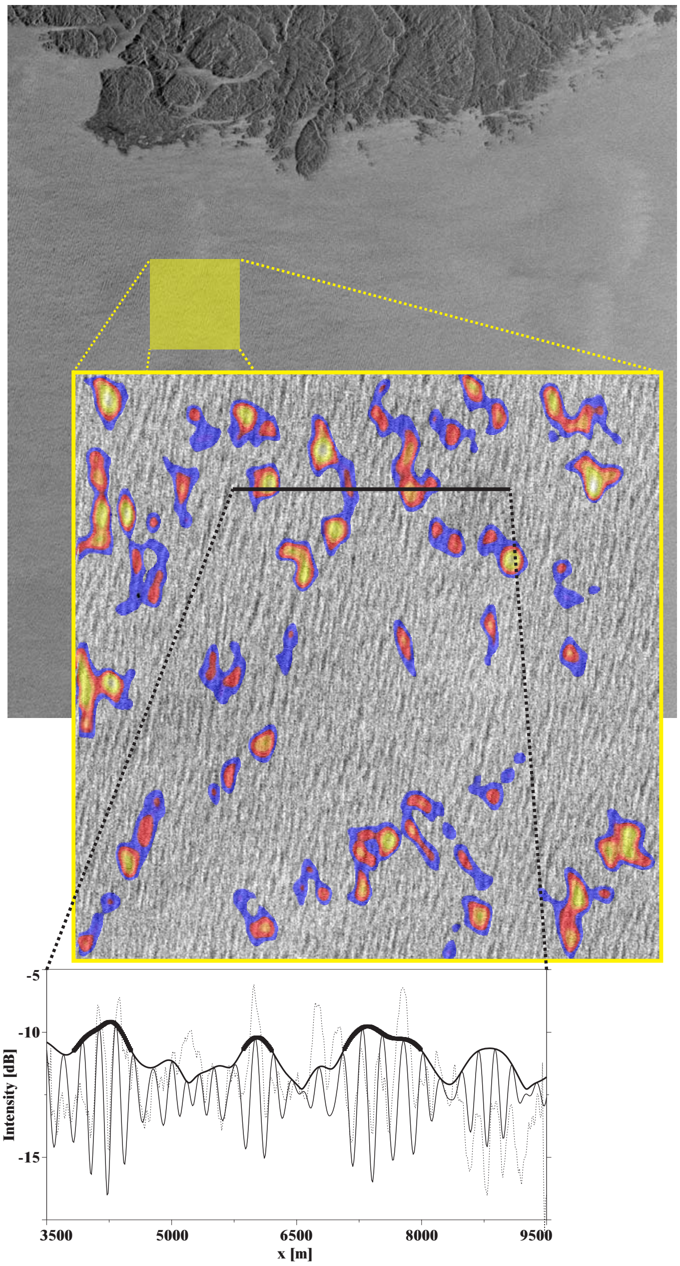

Fig. 4. SAR image taken by the ERS-1 satellite at the south Norwegian coast on September 26, 1995. The image size is about 100 km × 100 km with a pixel size of 12.5 m. A sub image of about 12.8 km × 12.8 km has been extracted. It shows a range travelling ocean wave field. The selected dominant wave groups are transparently overlayed. A cut through the SAR image (black line in the sub image) is plotted. The thin dotted curve represents the intensity values from the SAR image, which were reduced for speckle. The band-pass filtered wave field is represented by the solid curve and the corresponding envelope function (bold curve) is overlayed. The selected groups are marked on the envelope.

wave groups. A cut through the SAR image (black line in the sub image) is plotted. The thin dotted curve represents the intensity values from the SAR image, which were reduced for speckle. The band-pass filtered wave field is represented by the solid curve and the corresponding envelope function by the bold curve. Several dominant wave groups are visible. These wave groups were selected by the algorithm and marked on the envelope.

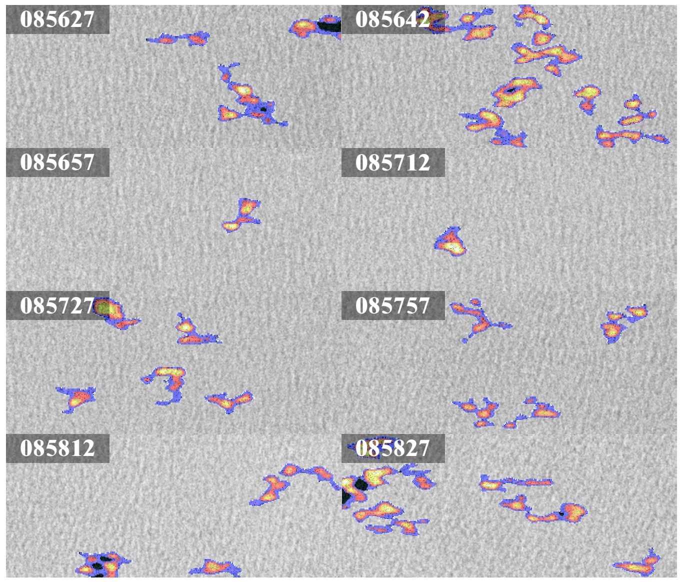

Fig. 5. 8 Imagettes recorded by the ASAR (advanced SAR) of the ENVISAT satellite launched in February 2002. The image size is about 5 km × 10 km with a pixel size of 5 m × 20 m. The imagettes show range travelling ocean wave fields. The selected dominant wave groups are transparently overlayed.

The second data set is a set of imagettes, available from the ASAR (advanced SAR) of the ENVISAT satellite launched in February 2001. The dimensions are 5 km × 10 km with a pixel size of 5 m × 20 m. In Fig. 5, eight examples of the analyzed imagettes are shown. The imagettes show range travelling ocean wave fields as well as the SAR image. To retrieve wave groups the imagettes have been processed with the algorithm. The selected dominant wave groups are transparently overlayed.

The wave groups in fig. 4 and 5 show preferred directions along which the wave groups are lined up. Their distributions in space may therefore deviate from a random selection. The wave numbers for the individual groups are well defined in components along travel directions $k_{\|}$ and perpendicular to travel direction $k_{\perp}$ (The authors define the travel direction perpendicular to the crest and through directions and resolve the 180° ambiguity by inspecting weather charts, which show winds from westerly directions). That means, it can be concluded quantitatively the travel speed C_g of the groups from

$$C_g = \omega / k_{\|} \tag{10}$$

where ω results from the deep water dispersion relation

$$\omega = g(k_{\|}^2 + k_{\perp}^2)^{0.5}. \tag{11}$$

From equation 10 it follows that the groups travel with the theoretical group velocity or faster, a result that will be taken up again in chapter V.

V. Results from Radar-Image Sequences

Using radar-image sequences the behavior of wave groups in space and time can be studied in the temporal and spa-

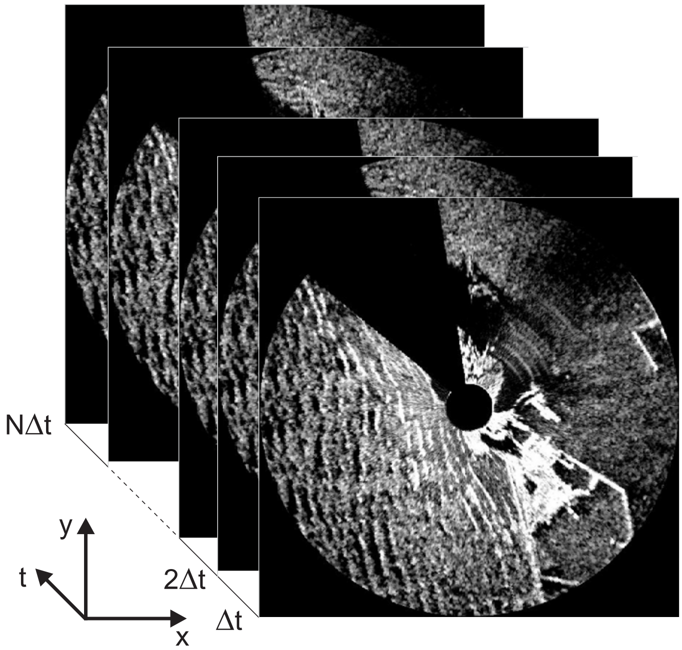

Fig. 6. Image sequence of the radar backscatter digitized by the Wave Monitoring System (WaMoS II) at the island of Helgoland (Germany). The backscatter signal is recorded spatially and temporally. The sampling period Δt per image is approximately 2 s.

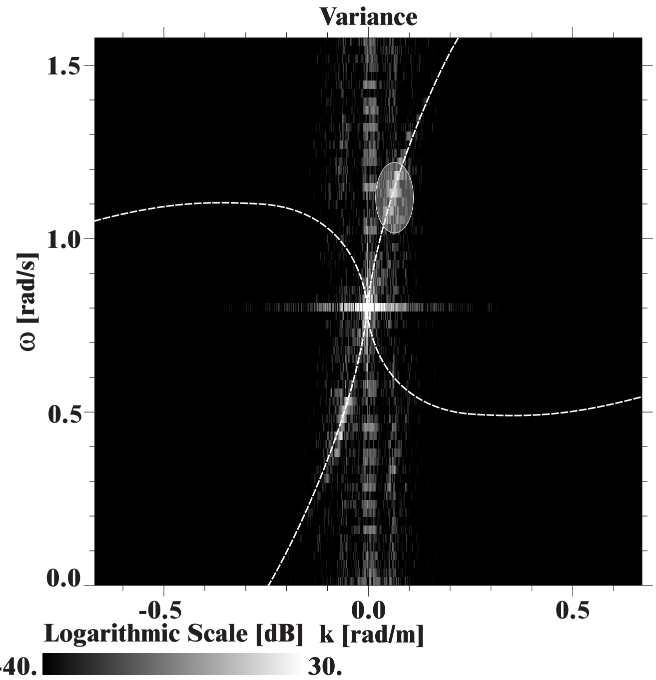

Fig. 7. Wave number-frequency slice trough the variance of the three dimensional spectrum after applying a 3D-FFT to the image sequence. The dashed curves give the dispersion relation, whereby it's shape is changed due to near surface currents. Filtered are only the complex Fourier coefficients bounded by the ellipse. By eliminating the redundant part of the variance in the negative frequency domain the wave envelope is constructed.

tial domain. As an example the algorithm has been applied to two radar-image sequences acquired from tower-based stations in the North sea. Both image sequences have been recorded by the Wave Monitoring System (WaMoS II). WaMoS II utilizes a conventional marine X-band radar to measure the backscatter of the microwaves from the sea surface. The temporal sampling period, given by the antenna rotation period Δt, is approximately 2 s. One data set was recorded in a shallow water area with a variable water depth of about 10 m at the island of Helgoland, the other was recorded in deep water at the Ekofisk platform. The image sequence from Helgoland consists of 64 images, whereas the Ekofisk data set has 32 images. The data sets cover a total time period of 2 minutes and 1 minute, respectively. Again, the resolution of ≈ 10 m works as a low pass filter so that only waves longer than ≈ 30 m are imaged by the system.

In Fig. 6 the image sequence from Helgoland is shown. After transforming the image sequence into the wave number-frequency domain using a 3D-FFT one gets the variance (squared modulus) and the phase of the complex Fourier coefficients. Fig. 7 shows a wave number-frequency slice of the variance spectrum. The signal of the linear surface gravity waves, which is located on the dispersion relation (dashed curves) is filtered by multiplying the complex spectrum with the normalized 3D-Gabor filter. Only the complex coefficients in the positive frequency domain are selected (area bounded by ellipse). The image transfer function is applied with the given significant wave height to convert the given image spectrum into a wave spectrum. After back transformation of the remaining Fourier coefficients in the wave number-frequency domain with an inverse 3D-FFT into the spatio-temporal domain, the complex envelope function of the dominant surface waves is spatially and temporally determined.

By applying a threshold on the envelope amplitude the dominant wave groups are selected. Fig. 8 shows the results of both analyzed cases, with the shallow water case from Helgoland (top) and the deep water case from Ekofisk (bottom). The static pattern has been removed from the images to make the imaged waves clearer. Transparently superimposed are the wave envelopes of the dominant wave groups. All the retrieved areas are counted and measured here in regard to the area size. Fig. 9 gives the relation between threshold level and total area size for each inverted image of the image sequence from Ekofisk. For each threshold level the area size is similar over the image sequence because the groups are not disintegrating in deep water due to dispersion.

The speed of wave groups, defined by the velocity of the "gravity" center of energy of the selected propagating envelope surface weighted by the potential energy ρ^2, which is termed group velocity C_g is given for one dimensional cases by:

$$C_g = \frac{1}{2}[1 + \frac{2kd}{\sinh 2kd}]C, \tag{12}$$

with C the phase velocity of the individual waves, which is defined as ωk^{-1}, the water depth d and wave number k. In deep water the term $(2kd)/(\sinh 2kd)$ is approximately

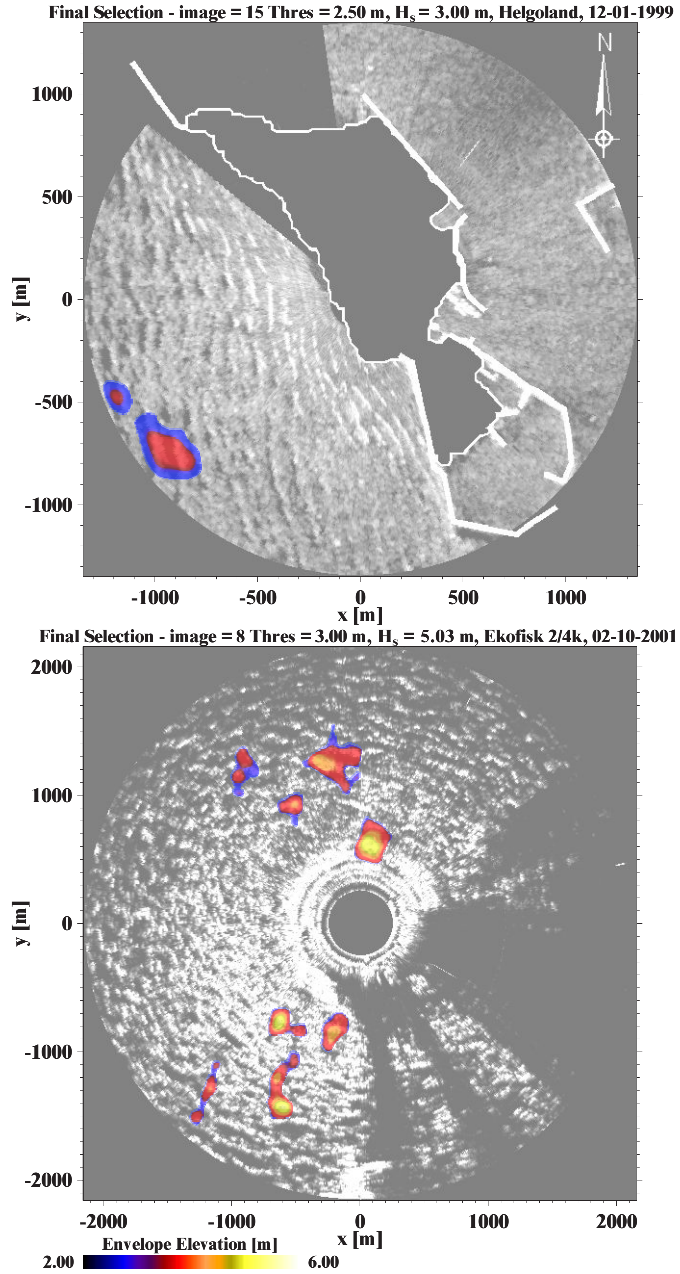

Fig. 8. Sample images of the image sequences from Helgoland (above) and Ekofisk (below). After applying the method one get the dominant wave groups. The static pattern has been removed from the images to make wave patterns more clear. Transparently overlayed are the wave envelopes of the dominant wave groups with a chosen minimum area size.

zero, giving:

$$C_{g0} = \frac{1}{2}C \tag{13}$$

where the index 0 denotes deep water. In shallow water $\sinh(2kd) \approx 2kd$ and

$$C_{gs} = C \approx \sqrt{gd}, \tag{14}$$

with index s denoting shallow water. These equations have been used for a first comparison with the group velocities in two dimensions. The determination of the phase velocities

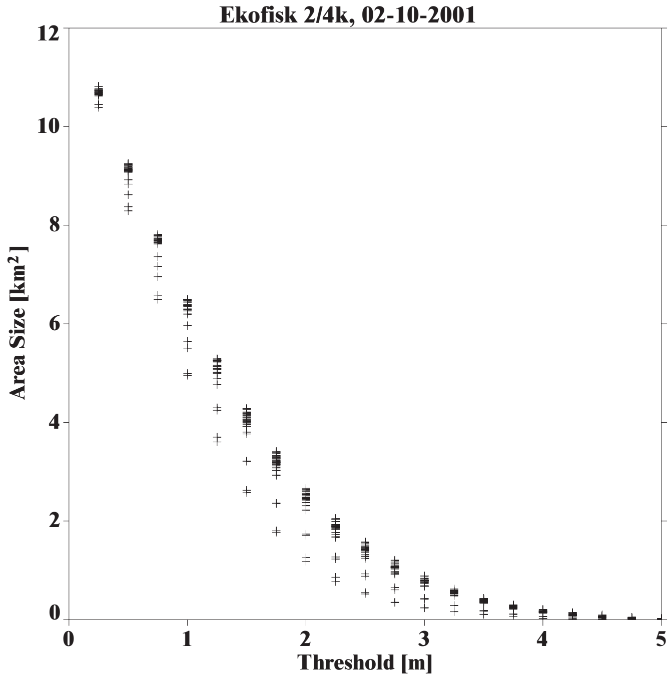

Fig. 9. Total wave group area size for various thresholds. Each threshold is applied to all inverted envelope images of a sequence. For each threshold level the area size is similar over the image sequence because the groups are not disintegrating in deep water due to dispersion.

of the individual waves is done using a differential-based motion estimation technique [17].

Fig. 10 shows the result for the deep water case from Ekofisk. The upper image shows the center of energy of all selected wave groups for the image sequence of Ekofisk with a threshold for wave envelope height of 3.00 m. Again, the center of energy is defined to be the "gravity" center of a wave group weighted by the potential energy ρ^2. The travel direction of all groups is varying, but goes in average with the main travel direction of the single waves. The lower plot shows the phase velocity of the single waves (dashed curve) and the group velocity (solid curve) with their mean values (top) for the highlighted wave group path. The lines give the velocities regarding the linear wave theory, which are determined with the frequency and wave number at the spectral peak. Phase and group velocity are oscillating around their theoretical values. The group velocity is in average higher. In Fig. 11 the same plots for the shallow water case from Helgoland are shown. Theoretically phase and group velocity have the same value in shallow water, but the measured average velocities differ from each other and, both, phase and group velocity, are oscillating over time. Sometimes the group velocity is higher, sometimes lower than the phase speed of the single waves. To give a first explanation of the physical processes behind this phenomenon one has to observe the moving single waves and the envelope function in the image sequences. Watching the animated single waves of the deep water case at Ekofisk, an observer can see waves that originate at the rear of a group, move forward through the group travelling

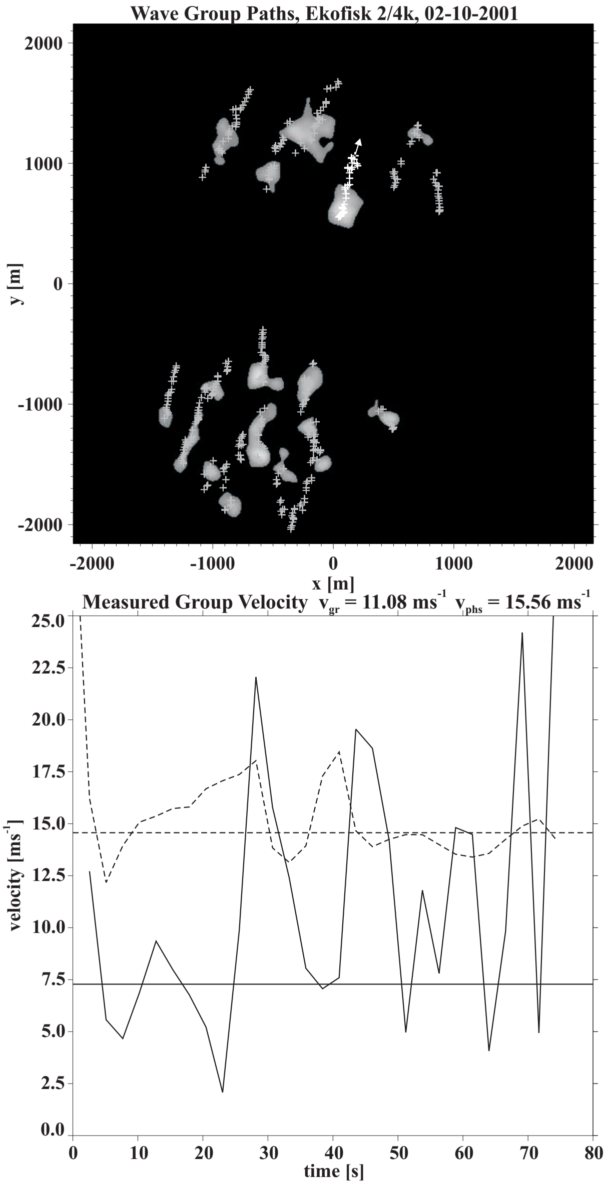

Fig. 10. The upper image shows the center of energy of all selected wave groups for the image sequence of Ekofisk with a threshold for wave envelope height of 3.00 m (white area). The center of energy is defined to be the "gravity" center of a wave group weighted by the potential energy ρ^2. The travel direction of all groups is varying, but goes in average with the main travel direction of the single waves. The lower plot shows the phase velocity of the single waves (dashed curve) and the group velocity (solid curve) with their mean values (top) for the highlighted wave group path. The lines give the velocities regarding the linear wave theory.

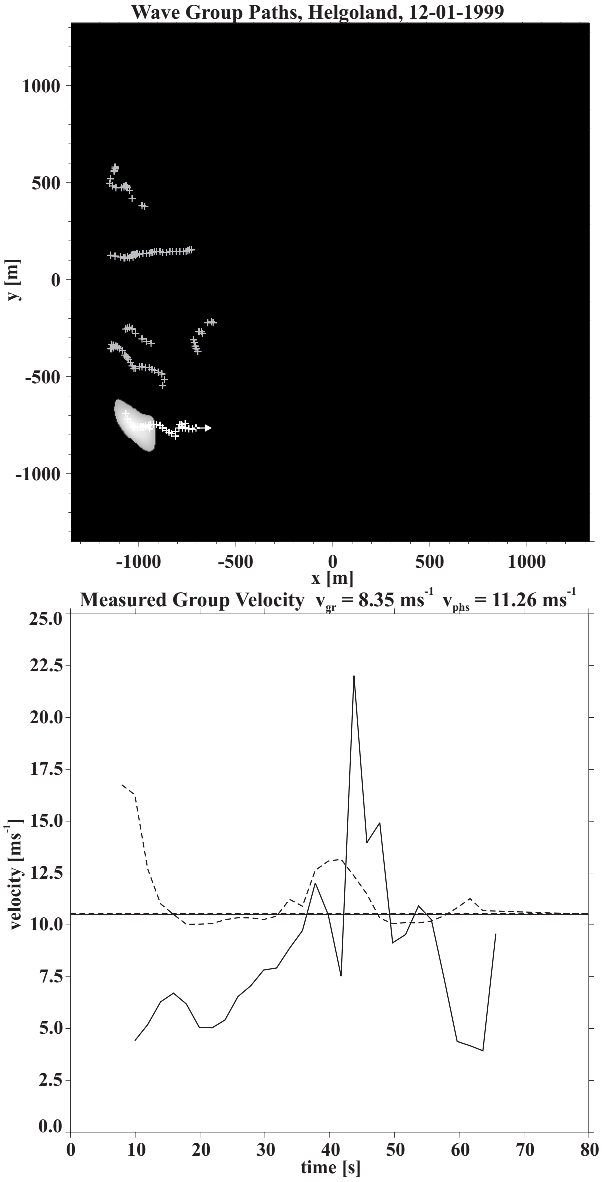

Fig. 11. The images show the same like Fig. 10 for the image sequence of Helgoland in a shallow water area with a threshold for wave envelope height of 2.50 m (white area). The travel direction of the groups is particulary strongly varying, but goes in average with the main travel direction of the single waves.

at phase velocity and disappear at the front of the group. These waves give an explanation for seemingly increasing and decreasing group velocities. Fig. 12 shows a sequence of six images of the modulus of complex envelope (amplitude) from the Helgoland data set. The images have a time difference of 10 s. The dashed lines mark a distance of 500 m and the arrow gives the travel direction of the dominant group in the images. The waves in this area are travelling in an easterly direction. Observing the wave envelope gives an energy transfer in two dimensions and therefore also addresses the wave crests. Determining the angle of the measured group-velocity vector validates the observation and shows that wave groups are, therefore, not only travelling with the waves. Furthermore, one can see how the wave group is developing and is varying in both amplitude and horizontal dimensions. A transversal modulation of the wave groups by other waves systems might be an explanation. The 2d change in size of the wave groups is especially interesting because it may be correlated with the background horizontal currents in the area [18].

VI. Conclusions

Properties of individual wave groups in single radar images as well as radar-image sequences have been stud-

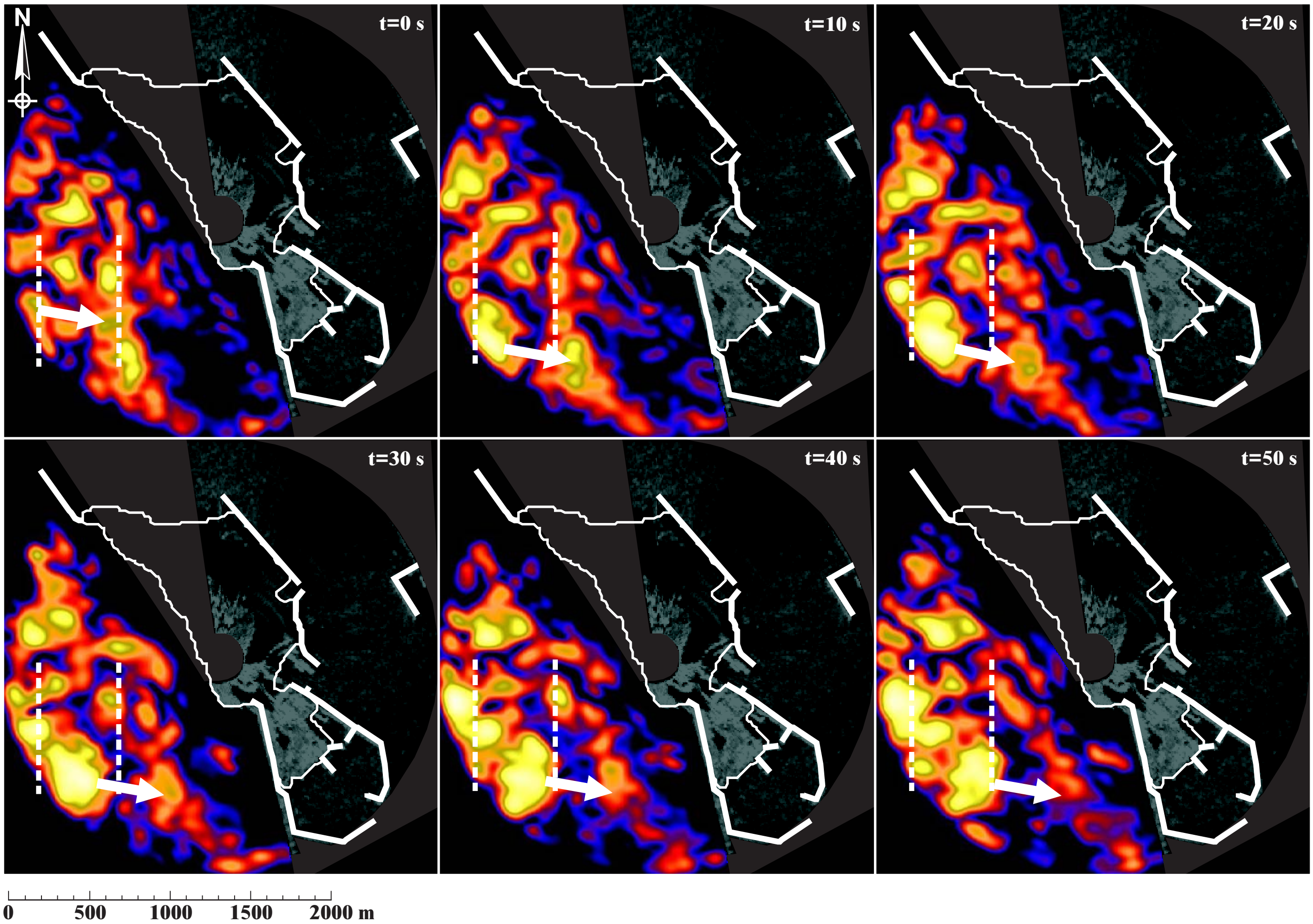

Fig. 12. Sequence of six images from Helgoland of the modulus of the complex envelope function after applying a inverse 3d-FFT to the filtered complex Fourier coefficients of the wave number-frequency spectrum. The images have a time difference of 10 s. The dashed lines mark a distance of 500 m and the arrow gives the travel direction of the dominant group in the images.

ied. This was possible by the quantitative measurement and analysis of wave groups both spatially and spatial-temporally. An image or image sequence of linear surface gravity waves is band-pass filtered and the temporal envelope was defined at each point. The filtering and determination of the complex envelope function are performed in the Fourier domain. The radar-image sequences are inverted to give the 2d sea-surface elevation. The retrieved groups are investigated with regard to their area size and maximum amplitude.

A SAR image acquired by the European satellite ERS-1, imagettes from the European satellite ENVISAT and image sequences recorded using a conventional nautical radar have been analyzed. The SAR image has been recorded at the south-west coast of Norway and the ENVISAT imagettes are first examples from the ocean surface. The radar-image sequences are from two different locations, one from a shallow water area at the island of Helgoland and the other one from a deep water area at the Ekofisk platform. It was possible to determine location and size of wave groups from SAR imagery. The large coverage of SAR images, together with their high resolution, provide valuable information about the distribution and size of wave groups. Radar-image sequences, collected with the WaMoS system, allow the measurement of the spatial and temporal development of wave groups, their extension and velocities, which has been done here. Comparison of measured wave group velocities in shallow and deep water gives a deviation of the average value with the group velocities resulting from linear wave theory and shows a clear oscillation of the group velocities in 2d.

Overall, the application of the algorithm on SAR images and the results from nautical radar-image sequences show the applicability of these data for detection and measuring of wave groups in spatial and temporal dimensions.

In the next step the physics behind the phenomenon of oscillating group velocity and energy transfer along the wave crest is further investigated.

Acknowledgement

This work was carried out in the frame work of the European project MAXWAVE (project no.: evk: 3-2000-00544). The authors would like to thank the European Space Agency (ESA) for the ERS SAR data in the framework of the ERS-A0 COMPLEX. The radar-image sequences were kindly made available by the company OceanWaves.

References

[1] K. Trulsen, "Simulating the spatial evolution of a measured time series of a freak wave," in *Proc. Rogue Waves 2000*, Oslo, Norway, 2001, pp. 265–273.

[2] M.S. Longuet-Higgins, "The statistical analysis of a random moving surface," in *Phil. Trans. R. Soc. London A*, 1957, pp. 321–387.

[3] M.S. Longuet-Higgins, "Wave group statistics," in *E.C. Monahan and G. Mac Nioceill (eds.), Oceanic Whitecaps*, 1986, pp. 15–35.

[4] W. R. Alpers, D. B. Ross, and C. L. Rufenach, "On the detectability of ocean surface waves by real and synthetic aperture radar," *J. Geophys. Res.*, vol. 86, pp. 6 481–6 498, 1981.

[5] K. Hasselmann and S. Hasselmann, "On the nonlinear mapping of an ocean wave spectrum into a synthetic aperture radar image spectrum," *J. Geophys. Res.*, vol. 96, pp. 10 713–10 729, 1991.

[6] G. Engen and H. Johnson, "SAR-ocean wave inversion using image cross spectra," *IEEE Trans. Geosci. Rem. Sens.*, vol. 33, pp. 1047–1056, 1995.

[7] I.R. Young, W. Rosenthal, and F. Ziemer, "A threedimensional analysis of marine radar images for the determination of ocean wave directionality and surface currents," *J. Geophys. Res.*, vol. 90,C1, pp. 1049–1059, 1985.

[8] C.M. Senet, J. Seemann, and F. Ziemer, "The near-surface current velocity determined from image sequences of the sea surface," *IEEE Trans. Geosci. Remote Sens.*, vol. 39, pp. 492–505, 2001.

[9] K. Hessner J.C. Nieto Borge and K. Reichert, "Estimation of the significant wave height with x-band nautical radars," in *Proceedings of the 18th International Conference on Offshore Mechanics and Arctic Engineering (OMAE)*, St. John's, Newfoundland, Canada, 1999, number OMAE99/OSU-3063.

[10] L.B. Wetzel, "Electromagnetic scattering from the sea at low grazing angles," *Surface Waves and Fluxes, Geernaert and W.J. Plant (eds.), Kluwer Academic Publishers*, vol. II, pp. 109–171, 1990.

[11] S.O. Rice, "The mathematical analysis of random noise," in *Bell Systems Technical Journal*, 1944, vol. 23, pp. 282–332.

[12] S.O. Rice, "The mathematical analysis of random noise," in *Bell Systems Technical Journal*, 1945, vol. 24, pp. 46–156.

[13] J. Seemann, "Interpretation der struktur des wellenzahlfrequenzspektrums von radar-bildsequenzen des seegangs," in *Diss., GKSS Research Center*, University of Hamburg, Germany, 1997.

[14] J.C. Nieto Borge, G.R. Rodríguez, K. Hessner, and P.I. González, "Inversion of nautical radar images for surface wave analysis," *J. Atmos. and Ocean Tech.*, submitted 2002.

[15] W. R. Alpers and C. L. Rufenach, "The effect of orbital motions on synthetic aperture radar imagery of ocean waves," *IEEE Trans. Antennas Propagat.*, vol. 27, pp. 685–690, 1979.

[16] H.E. Krogstad, "A simple derivation of Hasselmann's nonlinear ocean-synthetic aperture radar transform," *J. Geophys. Res.*, vol. 97, pp. 2 421–2 425, 1992.

[17] B. Jähne, H. Haußecker, and Peter Geißler, *Handbook of Computer Vision and Applications*, Academic Press, 1999.

[18] K.B. Dysthe, "Refraction of gravity wave by weak current gradients," *J. Fluid. Mech.*, vol. 442, pp. 157–159, 2001.

Heiko Dankert received the Diploma degree in civil engineering from the University of Rostock, Rostock, Germany, in 2000.
He is currently a Research Scientist working in the European project MaxWave in the Coupled Modeling Systems group, GKSS Research Center, Geesthacht, Germany. In 1999, he joined GKSS while writing his Diploma thesis about the spatial analysis of diffraction of wave fields using optical-image sequences. In 2000, he was a Visiting Scientist at the National Cheng Kung University, Coastal Ocean Monitoring Center, Tainan, Taiwan, R.O.C. His research interests are the development of algorithms to extract marine parameters and wind fields from nautical radar-image sequences.

Jochen Horstmann received the Diploma degree in physical oceanography in 1997 and his PhD in earth sciences, in 2002, from the University of Hamburg, Germany. In 1995 he joined the Coupled Model System group, GKSS Research Center, Geesthacht, Germany. Since 2000 he has been a Research Scientist at the GKSS Research Center in the Institute for Coastal Research. In 2002 he was a Visiting Scientist at the John Hopkins University (JHU) Applied Physics Lab (APL), Maryland, and the National Oceanic and Atmospheric Administration (NOAA) National Environmental Satellite, Data, and Information Service (NESDIS), Washington DC, USA. His main research interests are in extraction of geophysical parameters from RAR, SAR as well as interferometric SAR.

Susanne Lehner studied mathematics at the University of Hamburg, received 1979 her MSc in applied mathematics at Brunel University, in Uxbridge UK, and received 1984 her PhD in Geophysics at the University of Hamburg. She was research scientist at the Max-Planck Institute for Climatology in Hamburg and joined 1996 the German Aerospace Center (DLR/DFD) in Oberpfaffenhofen. Currently she is research scientist in marine remote sensing at the Remote Sensing Technology Institute (DLR/IFM), working on the development of algorithms determining marine parameters from SAR.

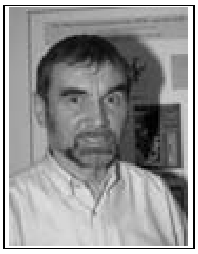

Wolfgang Rosenthal studied physics at Free University of Berlin, where he received in 1966 his Diploma degree and in 1972 his PhD in Theoretical Solid State Physics. He was research scientist at the Institute for Geophysics, Institute for Marine Research and at Max-Planck Institute for Meteorology at the University of Hamburg. In 1985 he joined the Institute for Coastal Research at GKSS Research Center working, working as research scientist in the boundary layer ocean-atmosphere branch.